System-Level Modeling and Virtual Testing of Fuel Cell Vehicle Mobypost Using Energetic Macroscopic Representation

Hao Bai
School of Automation, Northwestern Polytechnical University, Xi'an, China
hao.bai@nwpu.edu.cn

Chen Liu
School of Electrical Engineering, Zhengzhou University
chen.liu@zzu.edu.cn

Daniela Chrenko
FEMTO-ST Institute, Univ. Bourgogne Franche-Comté, UTBM, CNRS, Belfort, France
daniela.chrenko@utbm.fr

Alexandre Ravey
FEMTO-ST Institute, Univ. Bourgogne Franche-Comté, UTBM, CNRS, Belfort, France
alexandre.ravey@utbm.fr

Fei Gao
FEMTO-ST Institute, Univ. Bourgogne Franche-Comté, UTBM, CNRS, Belfort, France
fei.gao@utbm.fr

***Abstract*- Fuel cell vehicle (FCV) has drawn much attention due to its high efficiency, long drive range, and zero emission. The development of FCV involves complex architectures and requires an effective virtual testing methodology to improve R&D efficiency. Energetic Macroscopic Representation (EMR) is a graphical formalism to organize models and controls of multidisciplinary systems. It provides the seamless integrations of multi-level models and interconnections between virtual and real testing, which reduces the total development time of the electrified vehicles. Therefore, in this paper, the system-level model of FCV is designed using EMR for the high-fidelity virtual testing of electrified vehicles. An FCV Mobypost that is used for postal delivery in France is chosen as the studied vehicle. The virtual testing results are compared with the real testing. Good consistency is achieved, which validates the performances of the EMR-based FCV model in the virtual testing environment.**

I. Introduction

Air pollutant emissions from transport are one of the main concerns in controlling the air quality worldwide. Many countries are now searching for the electrified transportation solutions to protect the environment and alleviate air pollution. Fuel cell vehicle (FCV) is one of the promising alternatives of the internal combustion engine-powered vehicles to achieve electrified transportation due to its high efficiency, long drive range, and zero emission. FCV uses the fuel cell system in combination with a battery or a supercapacitor to provide power to the onboard electric drives. It involves multiple sources and multidisciplinary knowledge that requires efficient modeling architecture and high-fidelity virtual testing tools to improve development efficiency and reduce cost. The Energetic Macroscopic Representation (EMR) proposed in [1] is a unified modeling formalism that integrates multi-level models of components and connects virtual testing and real testing. EU H2020 PANDA project has the ambition of reducing the time-to-market of EVs by 20% through the EMR-based digital model architecture [2]. Therefore, the modeling and virtual testing of FCV using EMR is a viable solution to speed up its R&D and shrink its time-to-market.

Mobypost is an FCV developed in the EU project - *Mobility with Hydrogen for Postal Delivery* [3]. It is designed for ensuring the last step in the postal delivery process and delivers mails and parcels from local sorting centers to recipients. The hydrogen is locally produced by using the electric energy generated by photovoltaic technology to electrolyze water. Mobypost fulfills postal delivery cleanly and sustainably while providing a larger driving range than pure battery-powered vehicles. With the rapid process of the energy transition, there are growing needs for FCV like Mobypost, which brings mass production for the manufacturer and needs an effective tool to reduce the development and testing time. Therefore, in this paper, a system-level FCV model is developed using EMR formalism for the virtual testing of Mobypost. The modeling methodology and the EMR organization method are presented in detail. The developed Mobypost model is implemented in the Matlab/Simulink and simulated using a typical driving cycle in daily postal delivery. The simulation results are compared with the road testing results and the performances of the Mobypost EMR-based model are thus validated.

This paper is organized as follows. The components and system models of Mobypost in EMR are presented in Section II. The developed model is simulated and the results are compared with the real testing in Section III. The discussions and conclusions of this paper are given in Section IV.

II. Mobypost Modeling Using Energetic Macroscopic Representation

The basic structure of Mobypost is shown in Fig. 1 [4]. The Mobypost powertrain consists of a fuel cell stack followed by a DC-DC converter, a Li-ion battery pack directly connected to the DC link, two electric drives (e-drives) composed of two inverters, and two in-wheel permanent magnet synchronous motors (PMSM). There is no gearbox in Mobypost. The modeling of the Mobypost focuses on the fuel cell stack, the DC-DC converter, the Li-ion battery, the e-drives, and the

vehicle's motion model. Besides, an effective energy management strategy is applied to coordinate the operation of the fuel cell stack and battery pack. The essential parameters of fuel cell and battery are given in Table.1.

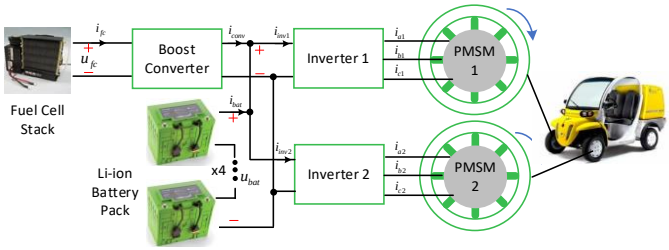

Fig. 1 FCV Mobypost powertrain structure [4].

TABLE I FUEL CELL AND BATTERY PARAMETERS

Fuel cell			
Fuel cell type	PEMFC	Number of cells	40
Nominal Power	1000 W	Active Area	61 cm^2
Stack Voltage Range	24-38 V	Nominal Stack Current	45 A
Batttery			
Battery Technology	Lithium-ion	Numbers of battery module	4
Nominal Module Voltage	12.8 V	Energy Density	89 Wh/kg
Nominal Capacity	110 Ah	Max. Continuous Load	150 A

A. Fuel cell model

A generic fuel cell model shown in Fig. 2 (a) is used in this paper [5]. The fuel cell is represented by a controlled voltage source in series with a resistor. E_{oc} is the open circuit voltage, N_c is the number of cells, A is the Tafel slope, i_0 is the exchange current, T_d is the response time, R_{fc} is the internal resistance, i_{fc} is the fuel cell output current, and u_{fc} is the fuel cell output voltage.

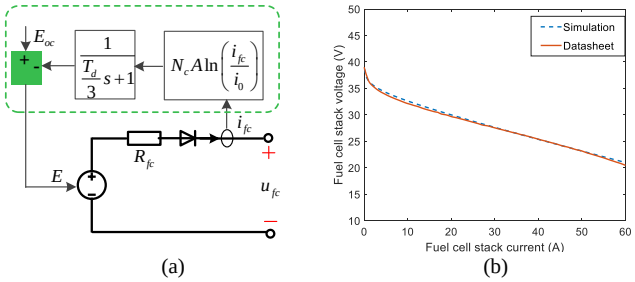

(a) (b)

Fig. 2 (a) Generic fuel cell model [5]; (b) Polarisation curve from datasheet and simulation results [6].

$$E = E_{oc} - N_c \cdot A \cdot ln\left(\frac{i_{fc}}{i_0}\right) \cdot \frac{1}{1/3 \cdot T_d s + 1} \quad (1)$$

$$u_{fc} = E - R_{fc} i_{fc} \quad (2)$$

The parameters of (1) and (2) can be approximated based on the data extracted from the polarization curve in the fuel cell datasheet [5]. Fig. 2 (b) shows the polarization curves obtained from the developed fuel cell model and the datasheet [6]. The simulated voltage-current relationship of the fuel cell is close to the experimental results, especially in the neighborhood of the nominal operating point.

B. Battery model

The battery model is composed of a controlled voltage source in series with a resistor [7], as shown in Fig. 3. The value of the voltage source depends on the battery SOC and can be represented by (3). E_0 is the battery constant voltage, K is the polarization voltage, C_{bat} is the battery capacity ($A \cdot h$), A is the exponential zone amplitude, and B is the inverse of the exponential zone time constant. The battery output voltage u_{bat} is thus expressed by (4) and SOC is computed by (5). The parameters are approximated based on the discharge and charge voltage profiles provided in the battery datasheet [7].

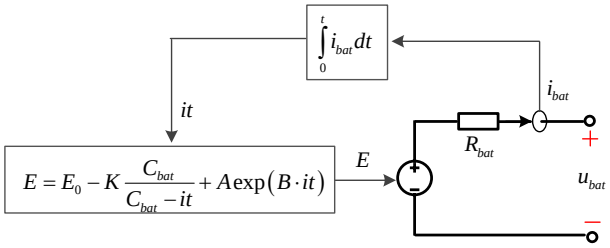

Fig. 3 Generic battery model [7].

$$E = E_0 - K\frac{C_{bat}}{C_{bat} - it} + Ae^{-B \cdot it} \quad (3)$$

$$u_{bat} = E - R_{bat} i_{bat} \quad (4)$$

$$SOC = \left(1 - \frac{\int i_{bat} dt}{3600 C_{bat}}\right) \times 100\% \quad (5)$$

C. DC-DC converter model

A boost converter shown in Fig. 4 (a) is used between the fuel cell stack and the DC link. A static model is applied to represent its behaviors [8]. The model is described by (6) and (7), where D is the duty cycle, and η_{conv} is the averaged efficiency of the power converter. The EMR of boost converter and its controller is illustrated in Fig. 4 (b).

$$L\frac{di_{fc}}{dt} = u_{fc} - u_{sw} \rightarrow i_{fc} = \int \frac{1}{L}(u_{fc} - u_{sw})\, dt \quad (6)$$

$$\begin{cases} u_{sw} = (1 - D) u_{bus} \\ i_{conv} = \eta_{conv}(1 - D) i_{fc} \end{cases} \quad (7)$$

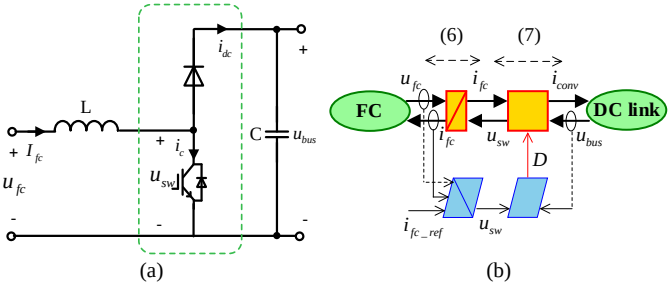

(a) (b)

Fig. 4 (a)Schematic diagram of boost converter; (b) EMR of boost converter

D. E-drive model

The e-drive of Mobypost includes a three-phase two-level inverter and an in-wheel PMSM. An averaged switch model is used to develop the inverter model. The averaged modulation function is defined by the ratio of phase-to-phase voltages to the DC link voltage, as given in (8). Therefore, the output voltages of the inverter are computed by (9).

$$\boldsymbol{m}_{inv} = \left[\frac{u_{ac}}{u_{bus}} \quad \frac{u_{bc}}{u_{bus}}\right]^T \tag{8}$$

$$\begin{bmatrix} u_a \\ u_b \\ u_c \end{bmatrix} = T_{l2p}\begin{bmatrix} u_{ac} \\ u_{bc} \end{bmatrix} = \frac{1}{3}\begin{bmatrix} 2 & -1 \\ -1 & 2 \\ -1 & -1 \end{bmatrix} u_{bus}\boldsymbol{m}_{inv} \tag{9}$$

A lumped parameter model in the d-q frame is used where the saturation and the cross-saturation effects are not considered. The Park transformation shown in (10) used in this paper is power-invariant, where ω_e is the electrical angular velocity, u_d, u_q are d, q axis voltages. The PMSM voltage equation is given by (11) using d, q axis currents i_d, i_q as the state variables [9]. R_S is the resistance of stator windings, λ_f is the stator flux linkage induced by the permanent magnets, and L_d , L_q are d, q axis inductances. Meanwhile, the electromagnetic torque can be computed by (12), where p is the number of pole pairs.

$$\begin{bmatrix} u_d \\ u_q \end{bmatrix} = \sqrt{\frac{2}{3}}\begin{bmatrix} cos(\omega_e t) & sin(\omega_e t) \\ -sin(\omega_e t) & cos(\omega_e t) \end{bmatrix}\begin{bmatrix} 1 & -\frac{1}{2} & -\frac{1}{2} \\ 0 & \frac{\sqrt{3}}{2} & -\frac{\sqrt{3}}{2} \end{bmatrix}\begin{bmatrix} u_a \\ u_b \\ u_c \end{bmatrix} \tag{10}$$

$$\begin{bmatrix} \frac{di_d}{dt} \\ \frac{di_q}{dt} \end{bmatrix} = \begin{bmatrix} L_d^{-1} & 0 \\ 0 & L_q^{-1} \end{bmatrix}\left(\begin{bmatrix} u_d \\ u_q \end{bmatrix} - \begin{bmatrix} R_S & 0 \\ 0 & R_S \end{bmatrix}\begin{bmatrix} i_d \\ i_q \end{bmatrix} - \begin{bmatrix} e_d \\ e_q \end{bmatrix}\right)$$

$$\text{Where } \begin{cases} e_d = -\omega_e L_q i_q \\ e_q = \omega_e\left(L_d i_d + \lambda_f\right) \end{cases} \tag{11}$$

$$T_e = p\left(\lambda_f i_q + \left(L_d - L_q\right) i_q i_d\right) \tag{12}$$

The e-drive model in EMR formalism is presented in Fig. 5. The PMSM torque control is realized based on the maximum torque-per-amp (MTPA) control algorithm by following the (13) [10], where i_m is the magnitude of armature current.

$$\begin{cases} i_d = \frac{\lambda_f}{4(L_q - L_d)} - \sqrt{\frac{\lambda_f^2}{16(L_q - L_d)^2} + \frac{i_m^2}{2}} \\ i_q = \sqrt{i_m^2 - i_d^2} \end{cases} \tag{13}$$

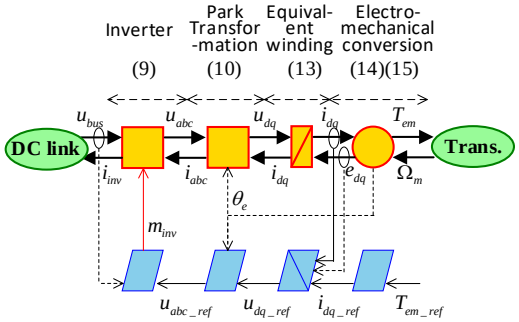

Fig. 5 EMR of e-drive.

E. Mobypost vehicle model

Due to the in-wheel PMSM used in Mobypost, the electromagnetic torque is directly deployed to the wheel. The traction force and rotating speed of the wheel can be computed by (14), where r_{wh} is the radius of the wheel. In the model, it is assumed that the wheels are not affected by slips and turns. Two sets of e-drive are used in Mobypost, and the driving forces of two wheels ($F_{wh1} + F_{wh2}$) are coupled with the braking force F_{br}. The total forces F_{tot} applied to the vehicle is computed by (15) and represented by a coupling element in EMR formalism.

$$\begin{cases} \Omega_{wh} = \Omega_m = \frac{v_{veh}}{r_{wh}} \\ F_{wh} = \frac{T_{em}}{r_{wh}} \end{cases} \tag{14}$$

$$F_{tot} = F_{wh1} + F_{wh2} + F_{br} \tag{15}$$

The vehicle velocity is thus obtained by (16), in which F_{res} is the resistive force to the motion and M_{veh} is the vehicle mass. An accumulation element represents the accumulation of the energy in the chassis.

$$v_{veh} = \frac{1}{M_{veh}}\int(F_{tot} - F_{res})dt \tag{16}$$

The road environment represents the resistive force F_{res} including the aerodynamic drag F_a, the rolling resistance F_r and the grading resistance F_g, as given in (17). F_a can be expressed by (18) where ρ is the air mass density, A_f is the equivalent front area of the Mobypost, C_d is the aerodynamic drag coefficient, and the v_{wind} is the wind speed. F_g and F_r can be obtained by (18), where the θ is the slope and C_r is the rolling resistance coefficient.

$$F_{res} = F_a + F_r + F_g \tag{17}$$

$$\begin{cases} F_a = \frac{1}{2}\rho A_f C_d (v_{veh} + v_{wind})^2 \\ F_g = M_{veh} g \sin\theta \\ F_r = C_r M_{veh} g \cos\theta \end{cases} \tag{18}$$

In EMR an inversion-based control scheme is used. Eq. (16) is inverted by a closed-loop control shown in (19), where *C(t)* is a PI controller in this paper.

$$F_{tot\_ref} = C(t)(v_{veh\_ref} - v_{veh}) + F_{res} \tag{19}$$

Eq. (15) is inverted using a distribution input k_{br} to distribute the forces between the brakes and the wheel, and a distribution input k_{di} to distribute the driving forces between two wheels.

F. Energy management strategy

Mobypost has two energy sources in the powertrain, i.e., fuel cell and battery, and needs an energy management system (EMS) to coordinate their operations. The EMS controls the start/stop of the fuel cell stack according to the battery SOC and sets the reference output power of the fuel cell stack. The rule-based energy management strategy is adopted in Mobypost and described by the flow chart in Fig. 6.

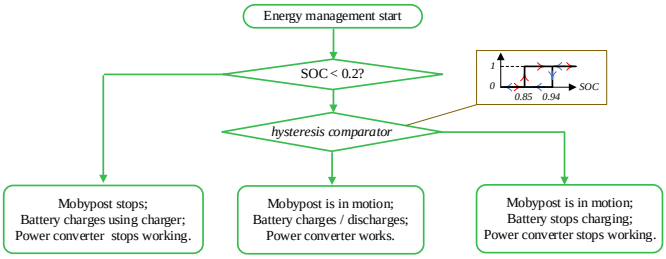

Fig. 6 Mobypost energy management strategy.

By integrating the models developed in Section II. A to Section II. F., the EMR of Mobypost can be organized by Fig. 7.

III. Simulation and Validation using Matlab-Simulink

The simulation is organized using the EMR formalism shown in Fig. 7. The driving cycle is collected based on the daily postal delivery track and treated as the input of the simulation. The references of the electromagnetic torque of two e-drives are derived base on the driving cycle. The fuel cell and battery are operating under the control of the energy management system. The EMR of Mobypost is implemented in Simulink environment and simulated with a 1ms time-step for the driving cycle from 0 to 10800s.

Fig. 8 to Fig. 12 demonstrate the simulation results of the Mobypost EMR model together with the results of the Mobypost on-road experiments. The dashed line is the simulation result and the solid line is the experimental result. Fig. 8 (a) depicts the vehicle speed curves and Fig. 8 (b) depicts the rotating speed of the in-wheel PMSM of the right wheel, where the magnified curves are plotted at the bottom. The Mobypost model follows the reference speed rapidly. The typical characteristics of the postal delivery driving cycle shown in Fig. 8 (a) contain many pauses, which provide the right time for the fuel cell to charge the battery to prolong the overall driving distance. Compared to the measured data, the simulation produces consistent results.

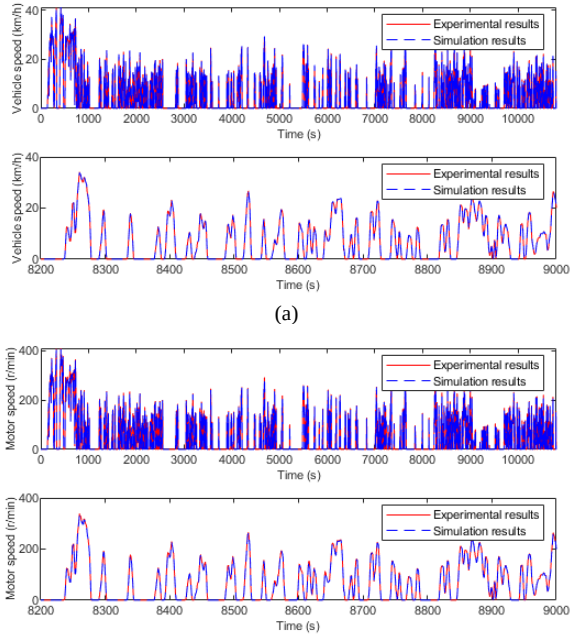

Fig. 8 (a) vehicle speed; (b) e-drive motor rotating speed.

The total power consumption of two e-drives is measured from the DC-link side in both experimental tests and simulation. The results are demonstrated in Fig. 9. The top sub-figure is the power consumption during the full tested driving cycle, the middle is the magnified waveforms between 8200 s and 9000 s to evaluate the performance of the developed model, and the bottom is the error between the measured results and

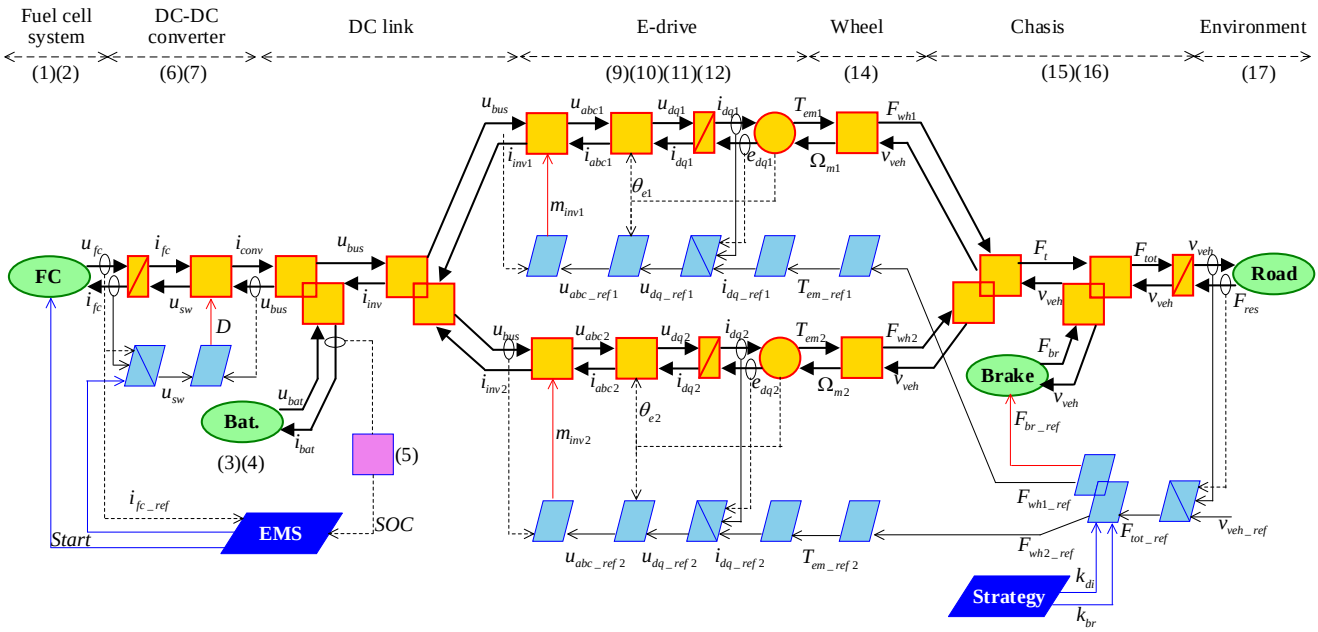

Fig. 7 EMR of Mobypost.

the simulated results for every time step in percentages which is calculated by (20). From the view of EMR, the developed model can accurately represent the realistic power demands of the Mobypost.

$$err = \left|\frac{Meas-Sim}{\max(Meas)}\right| \times 100\% \quad (20)$$

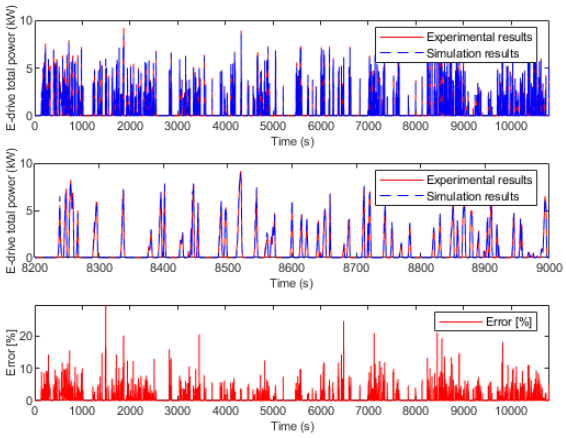

Fig. 9 Total power consumption of two e-drives measured in the DC side.

The operating principles of fuel cell and battery are presented in Fig. 6, in which the energy management is implemented using the rule-based strategy according to the battery SOC. The variations of battery SOC and H2 tank SOC during the whole driving cycle are shown at the top of Fig. 10 (a) and (b), while their errors are plotted at the bottom. The error between the measured and simulated SOC is calculated by (20).

In Fig. 10 (a), the simulated battery SOC shows accurate results and presents consistent variations with the measured one. The differences can also be observed. On the one hand, the sampling rate of the measured SOC is too slow, and some information of the Mobypost SOC is missing; on the other hand, the simulation errors of the power demands will be accumulated in the computation of SOC. Fig. 10 (b) depicts the results of the H_2 tank SOC. The simulation also produces accurate results. Errors occur in the period when the fuel cell stack is stopped. This is due to the power consumption of auxiliary devices in the fuel cell system, which is not considered in the simulation when the fuel cell is not working. In general, the SOCs of battery and H_2 tank in the developed model are accurate in the system-level simulation of Mobypost.

Fig. 11 shows the waveforms of fuel cell system output voltage, output current, and output power. The simulation results match the experimental results in the steady-state. The differences occur at the starting and stopping stages of the fuel cell. The start-up or shutdown of the fuel cell is determined by the EMS based on the battery SOC. Therefore, the exact time of the start-up and shutdown can be inaccurate due to the simulation errors of battery SOC. Moreover, the shutdown process of fuel cell involves a complex electrochemistry mechanism which is not considered in the system-level model developed in this paper. Nevertheless, the fuel cell model has satisfied accuracy regarding the system-level performance.

Fig. 12 presents the variations of the battery output power in the tested driving cycle. Due to the errors of SOC estimation, the deviations occur in the fuel cell start-up and shutdown processes. The steady-state simulation results are accorded with the experiments. The developed model follows the real power consumption of the vehicle's acceleration and deceleration. The slight differences can be observed in different driving conditions because the models of the power converters, e-drive, and fuel cell system use the averaged efficiencies to represent the power losses in each component.

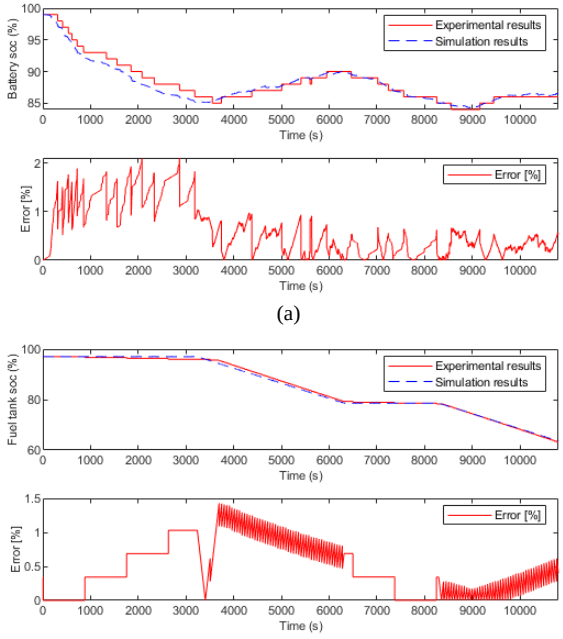

Fig. 10 (a) Battery SOC; (b) H2 tank SOC

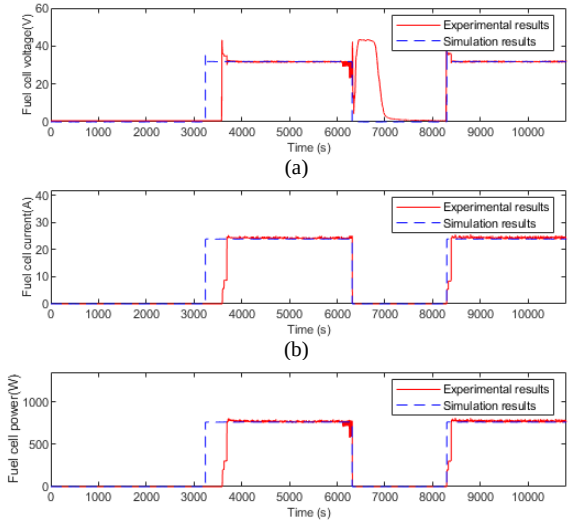

Fig. 11 Fuel cell system (a) output voltage, (b) output current, (c) output power.

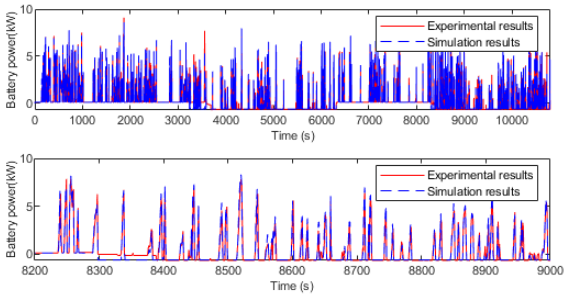

Fig. 12 Battery output power.

IV. Conclusions

This paper presents the virtual testing of the FCV with validation. The concept of the FCV and the tested FCV Mobypost that is developed for daily postal delivery applications are briefly described. The components in FCV including the fuel cell, the battery, the DC-DC converter, and the e-drive system are modeled and organized using the EMR formalism. These components' models are connected to compose the FCV model to be implemented in the virtual testing of the FCV.

Mobypost was tested in a three-hour driving cycle to cover the most use cases of postal delivery. The simulation was implemented in the Matlab-Simulink environment. The simulation results were compared with the measurements from the tests. The system-level behaviors of the Mobypost were accurately simulated, in terms of the current, the voltage, the power, the SOCs of the H_2 tank and the battery, the power demands of e-drives, and the vehicle's dynamic motion. The developed model is thus validated and proved to be credible in virtual testing.

The EMR modeling architecture enables the developed FCV model to be used in other simulation software. The parameters required in the Mobypost model are available in the vehicle development stages and don't involve complicated identification processes. The developed FCV model in this paper provides an efficient tool for the system/component design and testing, which is very favorable to reduce the development cost using the "W-model" concept proposed in PANDA [2].

Acknowledgment

This work was supported by European Commission H2020 grant PANDA (grant no. H2020-LC-GV-2018), EU grant no. 824256.

References

[1] A. Bouscayrol, J. P. Hautier, B. Lemaire-Semail, "Graphic Formalisms for the Control of Multi-Physical Energetic Systems", Systemic Design Methodologies for Electrical Energy, tome 1, Analysis, Synthesis and Management, Chapter 3, ISTE Willey editions, October 2012, ISBN: 9781848213883.

[2] A. Bouscayrol, A. Lepoutre, C. Irimia, C. Husar, J. Jaguemont, A. Lièvre, C. Martis, D. Zuber, V. Blandow, F. Gao, W. Van Dorp, G. Sirbu, J. Lecoutere, "Power Advanced N-level Digital Architecture for models of electrified vehicles and their components", Transport Research Arena 2020, Helsinki (Finland), April 2020.

[3] Mobility with Hydrogen for Postal Delivery, EU Project, GA#256834, website [Online] Available:http://mobypost-project.eu/.

[4] A. Ravey, S. Faivre, C. Higel, F. Harel and A. Djerdir, "Energy management of fuel cell electric vehicle with hydrid tanks," IECON 2014 - 40th Annual Conference of the IEEE Industrial Electronics Society, Dallas, TX, 2014, pp. 3962-3967.

[5] S. N. M., O. Tremblay and L. Dessaint, "A generic fuel cell model for the simulation of fuel cell vehicles," 2009 IEEE Vehicle Power and Propulsion Conference, Dearborn, MI, 2009, pp. 1722-1729.

[6] MES S.A., "DEA 1.0 Fuel Cell system datasheet," SW, Jan. 2012.

[7] O. Tremblay, L. Dessaint and A. Dekkiche, "A Generic Battery Model for the Dynamic Simulation of Hybrid Electric Vehicles," 2007 IEEE Vehicle Power and Propulsion Conference, Arlington, TX, 2007, pp. 284-289.

[8] P. Delarue, A. Bouscayrol and E. Semail, "Generic control method of multileg voltage-source-converters for fast practical implementation," IEEE Transactions on Power Electronics, vol. 18, no. 2, pp. 517-526, March 2003.

[9] X. Chen, J. Wang, B. Sen, P. Lazari and T. Sun, "A High-Fidelity and Computationally Efficient Model for Interior Permanent-Magnet Machines Considering the Magnetic Saturation, Spatial Harmonics, and Iron Loss Effect," in IEEE Transactions on Industrial Electronics, vol. 62, no. 7, pp. 4044-4055, July 2015.

[10] S. Morimoto, M. Sanada and Y. Takeda, "Wide-speed operation of interior permanent magnet synchronous motors with high-performance current regulator," in IEEE Transactions on Industry Applications, vol. 30, no. 4, pp. 920-926, July-Aug. 1994.